Supporting Information

Stable Solid-State Potassium Metal Batteries Enabled by a $KB_{11}H_{14}·2Me_3NBH_3$ Complex Electrolyte

Guo-guo Zhang,[a] *Pengtao Qiu,* *,[a] *Jia-Xin Kang,*[a, b] *Zhiwei Lu,*[c] *An-qi Zhu,*[a] *Xiaohu Yu,*[d] *and Xuenian Chen**[a, c]

[a] Henan Key Laboratory of Boron Chemistry and Advanced Materials, School of Chemistry and Chemical Engineering, Henan Normal University, Xinxiang, Henan 453007, China.

[b] Department of Chemistry and Guangdong Provincial Key Laboratory of Catalytic Chemistry, Southern University of Science and Technology, Shenzhen 518055, China.

[c] College of Chemistry, Zhengzhou University, Zhengzhou, Henan 450001, China.

[d] Shaanxi Province Key Laboratory of Catalytic Fundamental & Application, Shaanxi University of Technology, Hanzhong 723000, China.

*Emails: xuenian_chen@zzu.edu.cn (X.C.) and qiupengtao@htu.edu.cn (P.Q.).

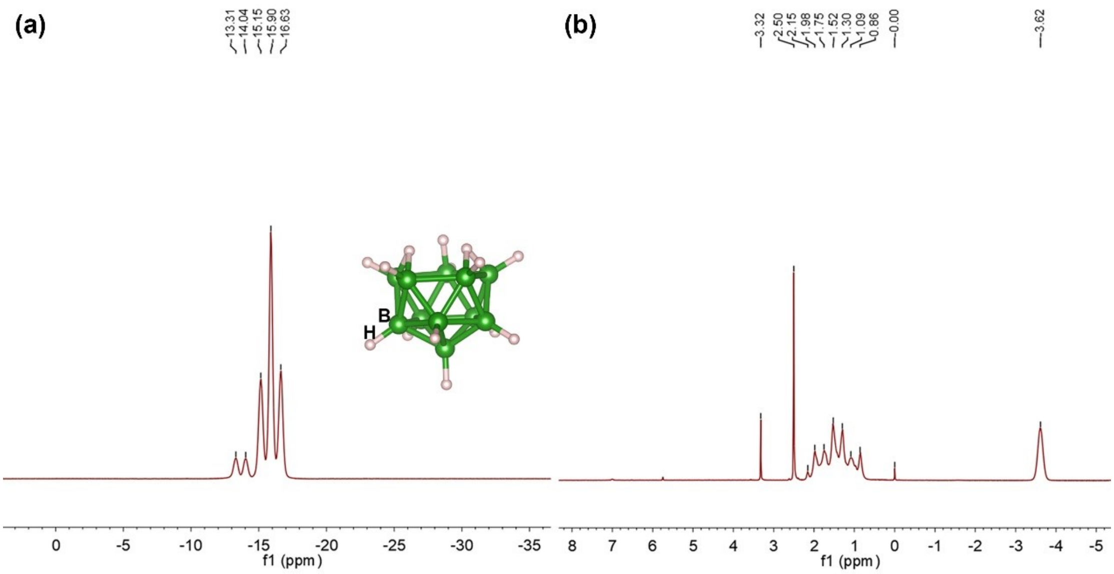

Fig. S1 (a) ^{11}B NMR and (b) ^{1}H NMR spectra of $KB_{11}H_{14}$ in DMSO-d$_6$.

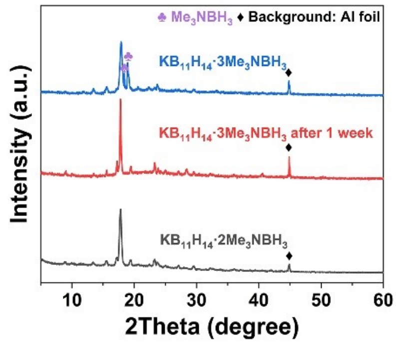

Fig. S2 XRD pattern of the $KB_{11}H_{14}\cdot 3Me_3NBH_3$ sample after standing one week at room temperature compared to those of the $KB_{11}H_{14}\cdot nMe_3NBH_3$ (n = 2 and 3) samples.

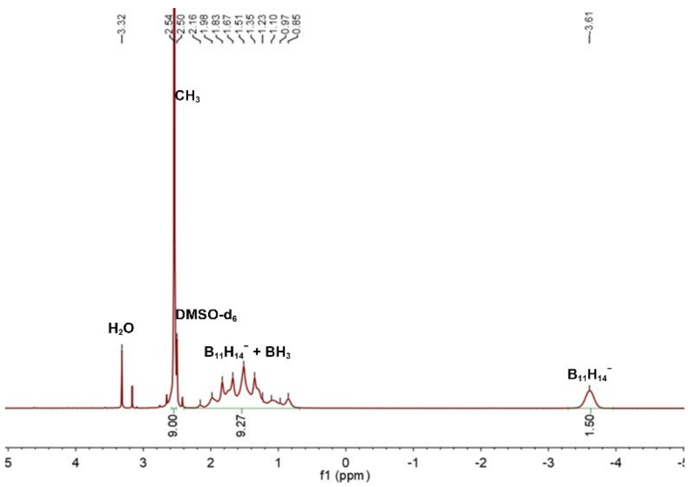

Fig. S3 ^{1}H NMR spectrum of $KB_{11}H_{14}\cdot 2Me_3NBH_3$ in DMSO-d$_6$.

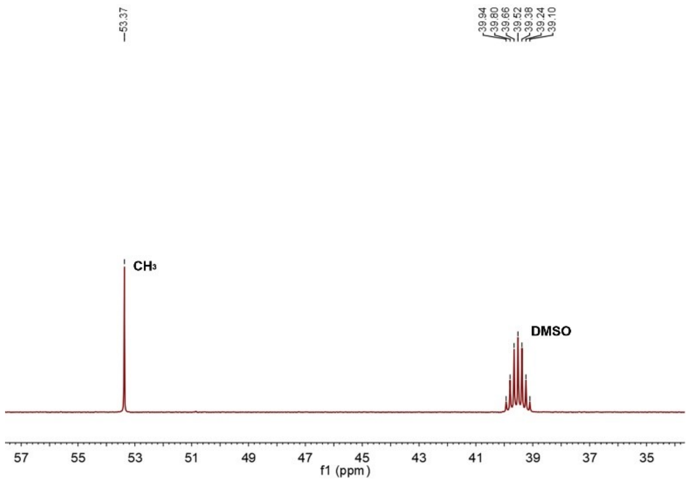

Fig. S4 ^{13}C NMR spectrum of $KB_{11}H_{14}$·$2Me_3NBH_3$ in DMSO-d_6.

Table S1. Crystallographic data for $KB_{11}H_{14}$·$2Me_3NBH_3$ and $KB_{11}H_{14}$.

	$\mathbf{KB_{11}H_{14}·2Me_3NBH_3}$	$\mathbf{KB_{11}H_{14}}$ [1]
Crystal system	Monoclinic	Triclinic
Space group	$P2_1/c$	*P*
T (°C)	25	25
a (Å)	7.0592	7.1950
b (Å)	20.1141	7.0462
c (Å)	12.4673	19.4087
α (°)	90.000	90.719
β (°)	106.645	94.045
γ (°)	90.000	89.971
V (Å^3)	1696.06	981.44

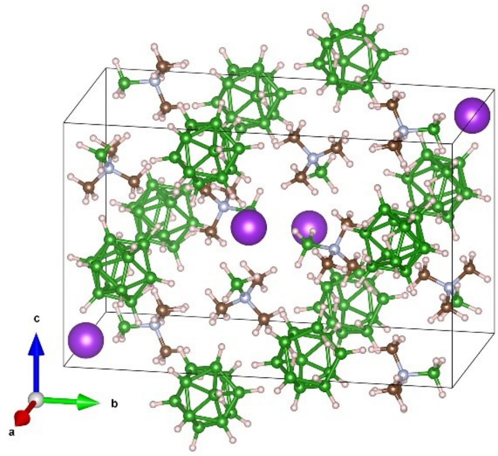

Fig. S5 Crystal structure of the $KB_{11}H_{14}·2Me_3NBH_3$ complex after the structure optimizations using the VASP package. Color scheme: K (purple), B (green), C (brown), N(white), and H (pink).

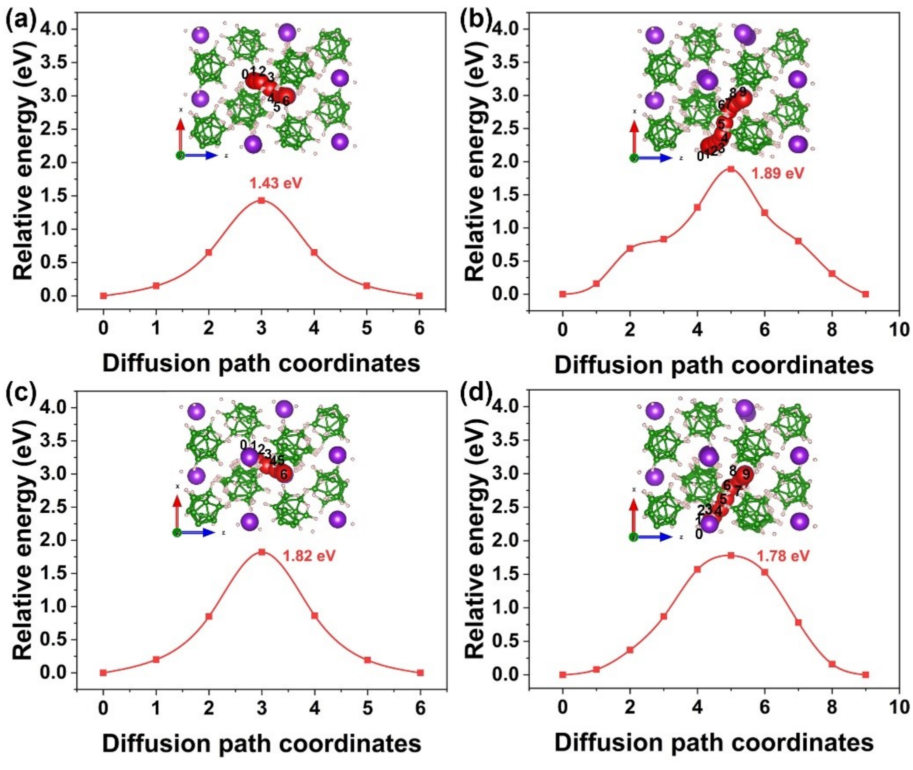

Fig. S6 Energy barriers of K^+ migration by the vacancy diffusion mechanism along other possible migration channels in a 2 × 2 × 1 supercell of $KB_{11}H_{14}$, insets: the migration channels. Color scheme: Framework K (purple), B (green), and H (pink).

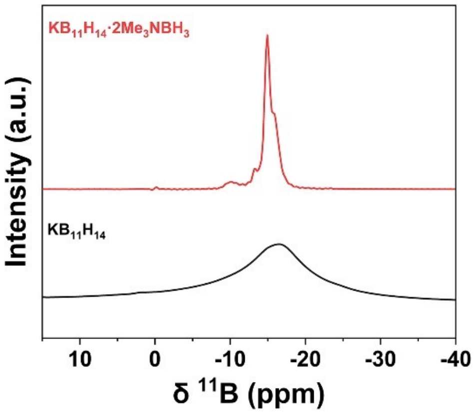

Fig. S7 Solid-state ^{11}B MAS NMR spectra of $KB_{11}H_{14}$ and $KB_{11}H_{14}{\cdot}2Me_3NBH_3$ at RT.

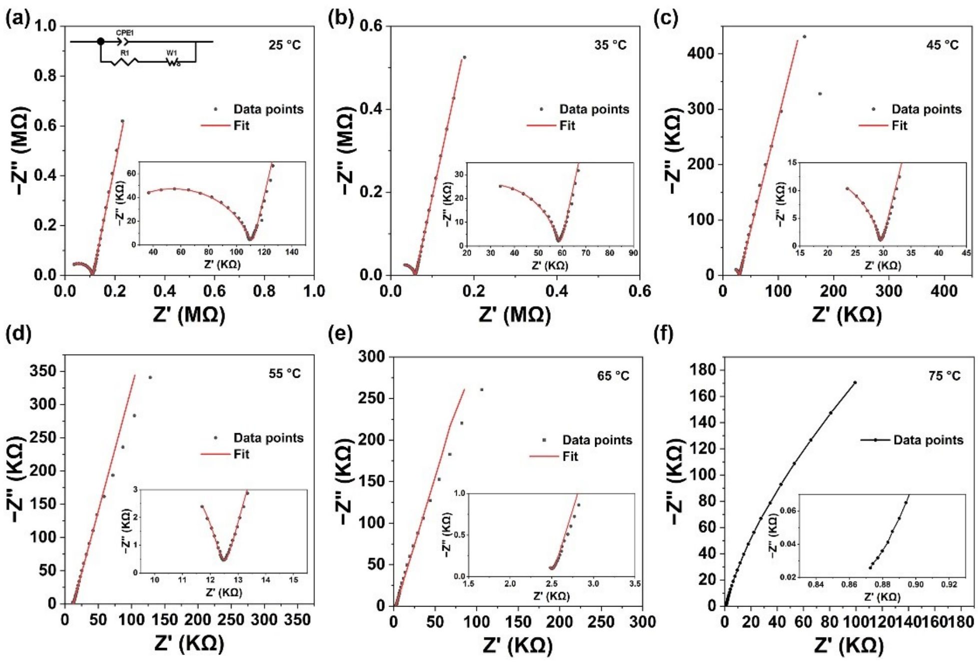

Fig. S8 (a-e) Nyquist plots of $KB_{11}H_{14}{\cdot}2Me_3NBH_3$ at different temperatures fitted with an equivalent circuit model (inset of a). (f) Nyquist plot at 75 °C, the intercept from Z′-axis was used to determine the value of resistance.

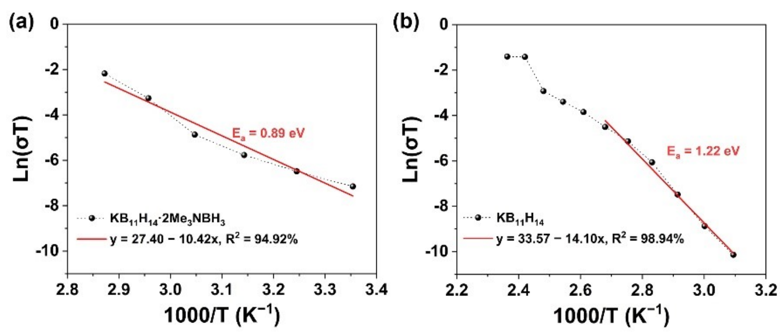

Fig. S9 The activation energies for K^+ diffusion in (a) $KB_{11}H_{14}{\cdot}2Me_3NBH_3$ and (b) $KB_{11}H_{14}$.

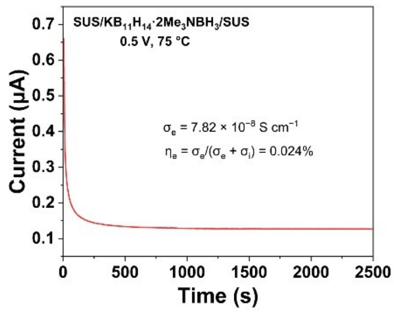

Fig. S10 CA curve of a SUS/$KB_{11}H_{14}$·$2Me_3NBH_3$/SUS cell under a voltage of 0.5 V at 75 °C.

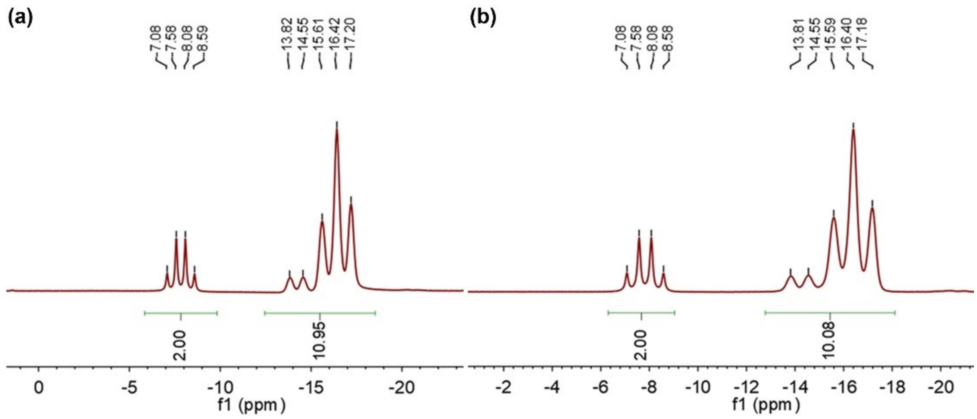

Fig. S11 ^{11}B NMR spectra of the $KB_{11}H_{14}$·$2Me_3NBH_3$ electrolytes after the LSV measurements within the potential windows of OCV to (a) 3.5 V and (b) 4 V at 45 °C.

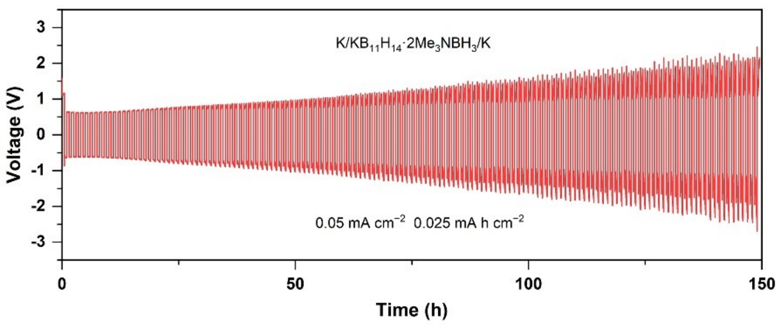

Fig. S12 Constant current GC curve of a K/$KB_{11}H_{14}$·$2Me_3NBH_3$/K cell at a current density of 0.05 mA cm^{-2}. Temperature: 45 °C.

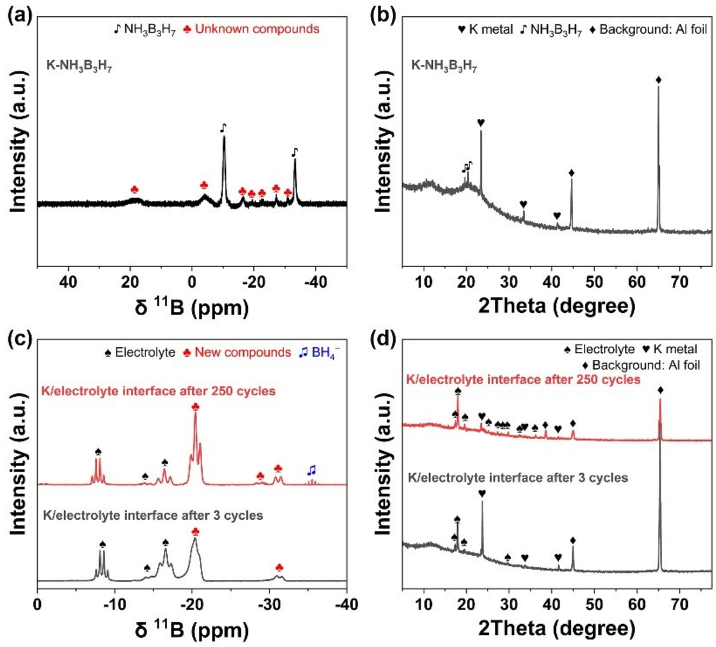

Fig. S13 (a) ^{11}B NMR and (b) XRD spectra of the preformed SEI layer in the K-$NH_3B_3H_7$ electrode. (c) ^{11}B NMR and (d) XRD spectra of the K/electrolyte interfaces in the symmetrical cell with the K-$NH_3B_3H_7$ electrodes after the given cycles.

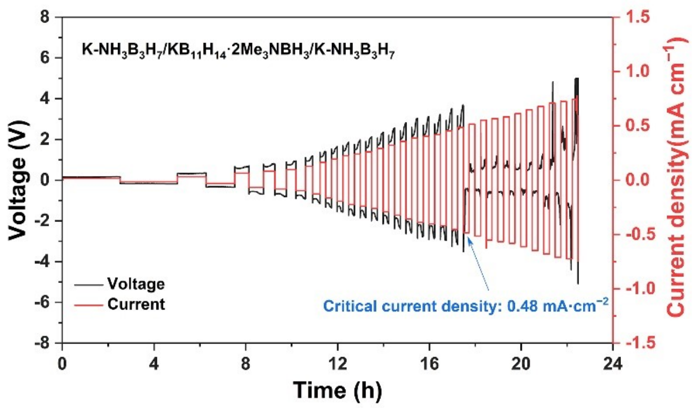

Fig. S14 Stepped current GC curve of the K-$NH_3B_3H_7$/$KB_{11}H_{14}$·$2Me_3NBH_3$/K-$NH_3B_3H_7$ cell. Temperature: 45 °C.

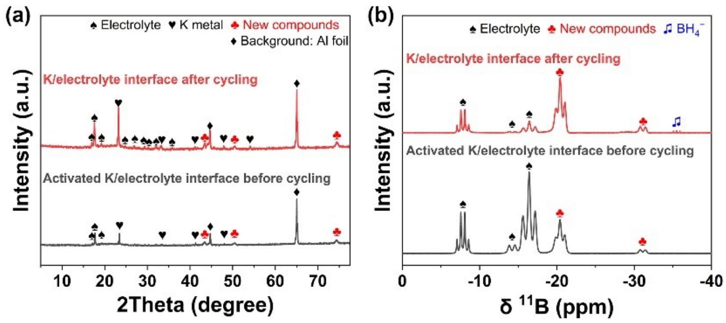

Fig. S15 (a) XRD and (b) ^{11}B NMR spectra of the K/electrolyte interfaces before and after galvanostatic charge/discharge cycling at 0.3 C.

Supplementary References

1. D. H. P. Souza, K. T. Moller, S. A. Moggach, T. D. Humphries, A. M. D'Angelo, C. E. Buckley and M. Paskevicius, Hydrated Alkali-$B_{11}H_{14}$ Salts as Potential Solid-State Electrolytes, *J. Mater. Chem. A,* 2021, **9**, 15027-15037.